# Bicritical scaling behavior in unidirectionally coupled oscillators

Sang-Yoon Kim* and Woochang Lim
*Department of Physics, Kangwon National University, Chunchon, Kangwon-Do 200-701, Korea*
(Received 3 September 2000; published 27 February 2001)

We study the scaling behavior of period doublings in a system of two unidirectionally coupled parametrically forced pendulums near a bicritical point where two critical lines of period-doubling transition to chaos in both subsystems meet. When crossing a bicritical point, a hyperchaotic attractor with two positive Lyapunov exponents appears, i.e., a transition to hyperchaos occurs. Varying the control parameters of the two subsystems, the unidirectionally coupled parametrically forced pendulums exhibit multiple period-doubling transtions to hyperchaos. For each transition to hyperchaos, using both a ''residue-matching'' renormalization group method and a direct numerical method, we make an analysis of the bicritical scaling behavior. It is thus found that the second response subsystem exhibits a new type of non-Feigenbaum scaling behavior, while the first drive subsystem is in the usual Feigenbaum critical state. The universality of the bicriticality is also examined for several different types of unidirectional couplings.

DOI: 10.1103/PhysRevE.63.036223 PACS number(s): 05.45.Jn

## I. INTRODUCTION

Many low-dimensional nonlinear systems exhibit period-doubling transitions to chaos. Using a renormalization group (RG) method, Feigenbaum had discovered universal scaling behavior near the accumulation point of the period-doubling cascade [1]. After that, efforts have been made in studies of coupled systems to attempt to generalize to high-dimensional nonlinear systems [2–9]. Here we are concerned with the critical scaling behavior of period doublings in unidirectionally coupled oscillators. These unidirectionally coupled systems have been used as models for open-flow systems [10]. In particular, they were actively discussed recently in relation to secure communication using chaos synchronization [11].

The coupled system investigated in this paper is two unidirectionally coupled parametrically forced pendulums (PFPs). For this unidirectionally coupled system, the drive subsystem acts on the response subsystem, while the response subsystem does not influence the drive one as in other unidirectionally coupled systems consisting of two Chua's circuits [12] and two Duffing oscillators [13]. Hence the two unidirectionally coupled PFPs have a skew product structure [14]. For a single PFP, vertical oscillation of its support leads to a time-periodic variation of its natural frequency [15]. As the amplitude of the vertical oscillation is increased, the lowest stationary point undergoes a cascade of ''resurrections,'' i.e., it becomes stabilized after its instability, destabilize again, and so forth *ad infinitum*. Recently, we have studied ''multiple period-doubling transitions to chaos,'' associated with such resurrections [16]. In each case of the resurrections, an infinite sequence of period-doubling bifurcations follows and leads to chaos. Consequently, an infinite series of period-doubling transitions to chaos occur successively with increasing amplitude. This is in contrast to the one-dimensional (1D) map [1], where only a single period-doubling transition to chaos occurs. However, the critical scaling behavior near each period-doubling transition point is the same as that for the 1D map.

Here we follow sequences of period doublings in two unidirectionally coupled PFPs by varying the two control parameters $A$ and $B$ of the two subsystems for a fixed value of the coupling parameter $C$. Scaling behavior is thus investigated near a bicritical point $(A_c, B_c)$ where two critical lines of period-doubling transitions to chaos in both subsystems meet. Note that this bicritical point corresponds to a border of chaos in both the subsystems. Hence, when crossing such a bicritical point, a hyperchaotic attractor with two positive-Lyapunov exponents [17] appears, i.e., a transition to hyperchaos occurs. With varying $A$ and $B$, the undirectionally coupled PFPs undergo a cascade of period-doubling transitions to hyperchaos. Using both renormalization group (RG) method and a direct numerical method, we investigate the bicritical scaling behavior for each transition to hyperchaos, and find that the response subsystem exhibits a new kind of non-Feigenbaum scaling behavior, while the drive subsystem is in the usual Feigenbaum's critical state. Note that this bicritical scaling behavior is the same as that in the two unidirectionally coupled 1D maps [7,8]. In addition, this kind of bicritical behavior was also observed in other systems consisting of unidirectionally coupled circuits [9]. Hence, such bicriticality may be a general phenomenon occurring in many unidirectionally coupled systems consisting of period-doubling subsystems.

This paper is organized as follows. We first introduce two unidirectionally coupled PFPs in Sec. II, and then discuss stability, bifurcations, and Lyapunov exponents. In particular, a convenient real quantity called the ''residue'' [18] is used to characterize stability of periodic orbits and their bifurcations. We then develop a ''residue-matching'' RG method, equating the residues of the orbit of level $n$ (period $2^n$) to those of the orbit of the next level $n+1$ in Sec. III. Using both residue-matching RG method and the direct numerical method, we investigate scaling behaviors near the bicritical points in Sec. IV and find a new kind of non-Feigenbaum scaling behaviors in the second response subsystem. To examine the universality of the bicriticality, sev-

*Electronic address: sykim@cc.kangwon.ac.kr

 

eral different types of unidirectional couplings are also studied. Finally, a summary is given in Sec. V.

## II. STABILITY, BIFURCATIONS, AND LYAPUNOV EXPONENTS

In this section, we discuss stability of period orbits in the four-dimensional (4D) Poincaré map of the two unidirectionally coupled PFPs, using the Floquet theory [19]. Bifurcations associated with the stability and Lyapunov exponents are also discussed.

A single PFP with a vertically oscillating support can be described by two first-order ordinary differential equations [15],

$$\dot{x}=y, \tag{1a}$$

$$\dot{y}=f_A(x,y,t), \tag{1b}$$

where $f_A(x,y,t)=-2\pi\beta\Omega y-2\pi(\Omega^2-A\cos 2\pi t)\sin 2\pi x$, $x$ is a normalized angle with range $x\in[0,1)$, the overdot denotes a derivative with respect to time $t$, $\beta$ is a normalized damping parameter, $\Omega$ is the normalized natural frequency of the unforced pendulum, and $A$ is the normalized driving amplitude of the vertical oscillation of the suspension point. Note that as a result of the vertical oscillation, the frequency of the pendulum varies periodically with time. Two identical PFPs are then coupled together with a unidirectional-coupling type to yield a skew-product system,

$$\dot{x}_1=y_1, \tag{2a}$$

$$\dot{y}_1=f_A(x_1,y_1,t), \tag{2b}$$

$$\dot{x}_2=y_2+C(x_2-x_1), \tag{2c}$$

$$\dot{y}_2=f_B(x_2,y_2,t)+C(y_2-y_1), \tag{2d}$$

where $A$ and $B$ are the normalized driving amplitudes of the vertical oscillations of the suspension points of the two PFPs and $C$ is a coupling parameter. For this unidirectionally coupled system, the first master PFP with state variables $x_1$ and $y_1$ can be regarded as a driving for the second slave or response PFP with state variables $x_2$ and $y_2$ through the coupling term. These unidirectionally coupled PFPs also have an inversion symmetry $S$ because the transformation

$$S: x_1\to -x_1,\ y_1\to -y_1,\ x_2\to -x_2,\ y_2\to -y_2 \tag{3}$$

leaves Eqs. (2) invariant. If an orbit $\mathbf{z}(t)[\equiv(z_1(t),z_2(t))]$, where $z_i=(x_i,y_i)$ $(i=1,2)$, is invariant under $S$, then it is called a symmetric orbit. Otherwise, it is called an asymmetric orbit and has its conjugate orbit $S\mathbf{z}(t)$.

The phase space of the two unidirectionally coupled PFPs is five dimensional with coordinates $x_1$, $y_1$, $x_2$, $y_2$, and $t$. Since the unidirectionally coupled PFPs are periodic in $t$, it is convenient to regard time as a circular coordinate (with mod 1) in the phase space. We then consider the surface of section, the $x_1$-$y_1$-$x_2$-$y_2$ hypersurface at integer times (i.e., $t=m$, $m$ is an integer). The phase-space trajectory intersects this hypersurface in a sequence of points. This sequence of points corresponds to a mapping on the 4D hypersurface. This map plot of an initial orbit point $\mathbf{z}(0)$ can be computed by stroboscopically sampling the orbit points $\mathbf{z}(m)$ at the discrete time $m$. We call the transformation $\mathbf{z}(m)\to\mathbf{z}(m+1)$ the Poincaré map, and write $\mathbf{z}(m+1)=P(\mathbf{z}(m))$. This 4D Poincaré map (with the inversion symmetry $S$) may have many attractors for fixed values of parameter values. For $A=B$ and $C=0$, it breaks up into two uncoupled identical two-dimensional (2D) maps possessing the inversion symmetry. If each uncoupled 2D map has either an asymmetric stable orbit $z\ [=(x,y)]$ or its conjugate orbit $z^*$, then the composite 4D map has one of the four pairs of orbits, $(z,z)$, $(z^*,z^*)$, $(z,z^*)$, and $(z^*,z)$. For the first and second (third and fourth) pairs, the 2D uncoupled maps have the same (different) kind of orbits. Hereafter, the corresponding pairs will be called the ''same (different) pairs.'' To classify the orbits in the composite 4D map, we should also take the phase shift between the uncoupled 2D maps into consideration. If each 2D map has a stable orbit of period $2^n$, then the composite 4D map has $2^n$ different states distinguished by the phase shift $N$ $(N=0,\ldots,2^n-1)$. Note that this multistability is preserved when the coupling is introduced, at least while its value is small enough. Hereafter, an orbit will be called an orbit of type $N_{s(d)}$ if it corresponds to the same (different) pair and there exists a phase shift $N$ between the state variables $z_1$ and $z_2$ of the first and second 2D maps [i.e., $z_1(m)=z_2(m+N)$] when we come to the point $C=0$ and $A=B$.

The linear stability of a $q$-periodic orbit of the 4D Poincaré map $P$, such that $P^q(\mathbf{z}(0))=\mathbf{z}(0)$, is determined from the linearized-map matrix $M\ [\equiv DP^q(\mathbf{z}(0))]$ of $P^q$ at an orbit point $\mathbf{z}(0)$. Here $P^q$ means the $q$-times iterated map. Using the Floquet theory [19], the matrix $M$ can be obtained by integrating the linearized differential equations for small perturbations with four initial perturbation $(\delta x_1,\delta y_1,\delta x_2,\delta y_2)=(1,0,0,0),(0,1,0,0),(0,0,1,0)$, and $(0,0,0,1)$ over the period $q$. Since the unidirectionally coupled system has a skew product structure [14], the linearized-map matrix $M$ has the following semiblock form:

$$M=\begin{pmatrix} M_1 & \mathbf{0} \\ M_3 & M_2 \end{pmatrix}, \tag{4}$$

where $\mathbf{0}$ is the $2\times 2$ null matrix. Hence, in order to determine the eigenvalues of $M$, it is sufficient to solve the eigenvalue problems of the two $2\times 2$ submatrices $M_1$ and $M_2$ independently. Here $M_1(A)$ and $M_2(B,C)$ determine the stability of the first drive and second response subsystems, respectively. Note also that the first submatrix $M_1$ is just the linearized Poincaré map of the PFP [16], and the coupling affects only the second submatrix $M_2$.

The eigenvalues $\lambda_{i,1}$ and $\lambda_{i,2}$ of $M_i$ $(i=1,2)$ are called the Floquet (stability) multipliers, which characterize the stability of the $i$th subsystem. Note also that the first pair of Floquet multipliers $(\lambda_{1,1},\lambda_{1,2})$ is just the pair of Floquet multipliers of the uncoupled PFP [16] and the coupling affects only the second pair of Floquet multipliers $(\lambda_{2,1},\lambda_{2,2})$. By

using the Liouville formula [20], we obtain constant Jacobian determinants $\mathcal{D}_1$ and $\mathcal{D}_2$ of the submatrices $M_1$ and $M_2$, respectively, where

$$\mathcal{D}_1 = e^{-2\pi\beta\Omega q}, \quad \mathcal{D}_2 = e^{-2(\pi\beta\Omega - C)q}. \tag{5}$$

Hence the $i$th pair of Floquet multipliers lies either on the circle of radius $\sqrt{D_i}$ or on the real axis in the complex plane. The periodic orbit becomes stable when all its four Floquet multipliers lie inside the unit circle in the complex plane (i.e., their moduli are less than unity). Here we consider the case of $\mathcal{D}_i<1$; $\mathcal{D}_1$ is always less than unity, while $\mathcal{D}_2$ becomes less than unity for $C<\pi\beta\Omega$. Then, the two pairs of Floquet multipliers never cross the unit circle in the complex plane except at the real axis, and hence Hopf bifurcations do not occur. Consequently, the stable periodic orbit can lose its stability only when a Floquet multiplier $\lambda_i$ passes through 1 or $-1$ on the real axis.

A more convenient real quantity $\mathcal{R}_i$ $(i=1,2)$, called the residue [18] and defined by

$$\mathcal{R}_i \equiv \frac{1+\mathcal{D}_i-\mathcal{T}_i}{2(1+\mathcal{D}_i)}, \tag{6}$$

is used to characterize the stability of periodic oscillations in the $i$th subsystem. Here $\mathcal{D}_i$ and $\mathcal{T}_i$ are the determinant and trace of the submatrix $M_i$, respectively. Then the Floquet multipliers $\lambda_i$ can be expressed in terms of $\mathcal{R}_i$ as follows:

$$\lambda_i = \frac{(1+\mathcal{D}_i)}{2}\{1-2\mathcal{R}_i \pm 2\sqrt{(\mathcal{R}_i-\mathcal{R}_{i,1}^*)(\mathcal{R}_i-\mathcal{R}_{i,2}^*)}\}, \tag{7}$$

where

$$\mathcal{R}_{i,1}^* = \frac{(1-\sqrt{\mathcal{D}_i})^2}{2(1+\mathcal{D}_i)}, \quad \mathcal{R}_{i,2}^* = \frac{(1+\sqrt{\mathcal{D}_i})^2}{2(1+\mathcal{D}_i)}. \tag{8}$$

For $\mathcal{R}_{i,1}^*<\mathcal{R}_i<\mathcal{R}_{i,2}^*$, Floquet multipliers occur in complex-conjugate pairs $(\lambda_i,\lambda_i^*)$ on the circle of radius $\sqrt{\mathcal{D}_i}$, while they come in real pairs $(\lambda_i,\mathcal{D}_i/\lambda_i)$ on the real axis for $\mathcal{R}_i<\mathcal{R}_{i,1}^*$ or $\mathcal{R}>\mathcal{R}_{i,2}^*$. Note also that the Floquet multipliers can cross the unit circle only at the real axis (i.e., at $\lambda_i=1$ or $-1$). For $\lambda_i=1$ and $-1$, the values of $\mathcal{R}_i$ are 0 and 1, respectively. Hence, when $0<\mathcal{R}_i<1$, the pair of Floquet multipliers $\lambda_i$ lies inside the unit circle. As $R_i$ decreases through 0 (i.e., a Floquet multiplier $\lambda_i$ increases through 1), the periodic orbit loses its stability via a saddle-node or pitchfork bifurcation. On the other hand, as $\mathcal{R}_i$ increases through 1 (i.e., a Floquet multiplier decreases through $-1$), it becomes unstable via a period-doubling bifurcation. For more detail on the bifurcations, refer to Ref. [21].

Finally, we briefly discuss Lyapunov exponents [22] of an orbit in the 4D Poincaré map $P$. The two submatrices $M_1$ and $M_2$ of $M$ determine Lyapunov exponents $(\sigma_{1,1},\sigma_{1,2})$ and $(\sigma_{2,1},\sigma_{2,2})$, characterizing the average exponential rates of divergence of nearby orbits in the first and second subsystems, respectively, where $\sigma_{i,1}\geq\sigma_{i,2}$ for $i=1,2$. Since the two submatrices have constant Jacobian determinants of Eq. (5), the two pairs of Lyapunov exponents satisfy $\sigma_{1,1}+\sigma_{1,2}=-2\pi\beta\Omega$ and $\sigma_{2,1}+\sigma_{2,2}=-2(\pi\beta\Omega-C)$. Note also that the first pair of Lyapunov exponents $(\sigma_{1,1},\sigma_{1,2})$ is just the pair of Lyapunov exponents of the uncoupled PFP [16] and the coupling affects only the second pair of Lyapunov exponents $(\sigma_{2,1},\sigma_{2,2})$.

## III. RESIDUE-MATCHING RENORMALIZATION GROUP METHOD

In this section, we develop a residue-matching RG method, equating the residues of the orbit of level $n$ (period $2^n$) to those of the orbit of the next level $n+1$. Note that this RG scheme can be easily applied to the 4D Poincaré map $P$ of the unidirectionally coupled PFPs.

The basic idea of the residue-matching RG method is to associate a value $(A',B')$ for each $(A,B)$ such that $P_{(A',B')}^{(n+1)}$ locally resembles $P_{(A,B)}^{(n)}$, where $P^{(n)}$ is the $2^n$th-iterated map of $P$ (i.e., $P^{(n)}=P^{2^n}$). Here $A$ and $B$ are the control parameters of the two subsystems, respectively, and the coupling parameter $C$ is fixed. A simple way to implement this idea is to linearize the maps in the neighborhood of their respective fixed points and equate the corresponding residues, characterizing their stability. This residue-matching RG method can be regarded as a generalized version of the eigenvalue-matching RG method, that has been successfully used in the two unidirectionally-coupled 1D maps [8]. Note also that the residue matching in slightly different contexts has been also used for the study of break-up of invariant circles in the area-preserving twist maps [23].

Consider two successive orbits of period $2^n$ and $2^{n+1}$, $\{\mathbf{z}(m)\}$ and $\{\mathbf{z}'(m)\}$, such that

$$\mathbf{z}(m) = P_{(A,B)}^{(n)}(\mathbf{z}(m)), \quad \mathbf{z}'(m) = P_{(A',B')}^{(n+1)}(\mathbf{z}'(m)), \tag{9}$$

where $\mathbf{z}=(z_1,z_2)$ and $z_i=(x_i,y_i)$. Here the state variable $z_1$ of the first subsystem depends only on $A$ but the state variable $z_2$ of the second subsystem is dependent on both $A$ and $B$. Linearizing $P^{(n)}$ and $P^{(n+1)}$ at $\mathbf{z}(m)$ and $\mathbf{z}'(m)$, respectively, we obtain

$$\begin{aligned} DP_{(A,B)}^{(n)} &= \prod_{m=1}^{2^n} DP_{(A,B)}(\mathbf{z}(m)), \\ DP_{(A',B')}^{(n+1)} &= \prod_{m=1}^{2^{n+1}} DP_{(A',B')}(\mathbf{z}'(m)), \end{aligned} \tag{10}$$

where $DP$ is the linearized Poincaré map of $P$. Then the eigenvalues of the linearized-map matrices, called the Floquet multipliers, determine the stability of the periodic orbits. However, as explained in Sec. II, it is more convenient to use the residues $\mathcal{R}_1$ and $\mathcal{R}_2$, defined in Eq. (6), to characterize the stability of periodic oscillations in the first and second subsystems, respectively. The recurrence relations for the old and new parameters are then given by equating the residues of level $n$, $\mathcal{R}_{1,n}(A)$ and $\mathcal{R}_{2,n}(A,B)$, to those of the next level $n+1$, $\mathcal{R}_{1,n+1}(A')$ and $\mathcal{R}_{2,n+1}(A',B')$, i.e.,

$$\mathcal{R}_{1,n}(A) = \mathcal{R}_{1,n+1}(A'), \tag{11a}$$

$$\mathcal{R}_{2,n}(A,B)=\mathcal{R}_{2,n+1}(A',B'). \tag{11b}$$

The fixed point $(A^*,B^*)$ of the renormalization transformation (11),

$$\mathcal{R}_{1,n}(A^*)=\mathcal{R}_{1,n+1}(A^*), \tag{12a}$$

$$\mathcal{R}_{2,n}(A^*,B^*)=\mathcal{R}_{2,n+1}(A^*,B^*). \tag{12b}$$

gives the bicritical point $(A_c,B_c)$, corresponding to a border of chaos in both subsystems, for a fixed $C$. By linearizing the renormalization transformation at the fixed point $(A^*,B^*)$, we obtain

$$\begin{pmatrix}\Delta A\\ \Delta B\end{pmatrix}=\begin{pmatrix}\left.\frac{\partial A}{\partial A'}\right|_* & \left.\frac{\partial A}{\partial B'}\right|_*\\ \left.\frac{\partial B}{\partial A'}\right|_* & \left.\frac{\partial B}{\partial B'}\right|_*\end{pmatrix}\begin{pmatrix}\Delta A'\\ \Delta B'\end{pmatrix} \tag{13}$$

$$=\Delta_n\begin{pmatrix}\Delta A'\\ \Delta B'\end{pmatrix}, \tag{14}$$

where

$$\Delta_n=\Gamma_n^{-1}\Gamma_{n+1}, \tag{15}$$

$$\Gamma_n=\begin{pmatrix}\left.\frac{d\mathcal{R}_{1,n}}{dA}\right|_* & 0\\ \left.\frac{\partial\mathcal{R}_{2,n}}{\partial A}\right|_* & \left.\frac{\partial\mathcal{R}_{2,n}}{\partial B}\right|_*\end{pmatrix}, \tag{16}$$

$$\Gamma_{n+1}=\begin{pmatrix}\left.\frac{d\mathcal{R}_{1,n+1}}{dA'}\right|_* & 0\\ \left.\frac{\partial\mathcal{R}_{2,n+1}}{\partial A'}\right|_* & \left.\frac{\partial\mathcal{R}_{2,n+1}}{\partial B'}\right|_*\end{pmatrix}, \tag{17}$$

where $\Gamma_n^{-1}$ is the inverse of $\Gamma_n$ and the asterisk denotes the fixed point $(A^*,B^*)$. After some algebra, we obtain the analytic formulas for the eigenvalues $\delta_{1,n}$ and $\delta_{2,n}$ of the matrix $\Delta_n$,

$$\delta_{1,n}=\frac{\left.\frac{d\mathcal{R}_{1,n+1}}{dA'}\right|_*}{\left.\frac{d\mathcal{R}_{1,n}}{dA}\right|_*}, \tag{18a}$$

$$\delta_{2,n}=\frac{\left.\frac{\partial\mathcal{R}_{2,n+1}}{\partial B'}\right|_*}{\left.\frac{\partial\mathcal{R}_{2,n}}{\partial B}\right|_*}. \tag{18b}$$

As $n\to\infty$, the eigenvalues of level $n$, $\delta_{1,n}$ and $\delta_{2,n}$ approach their limit values $\delta_1$ and $\delta_2$, which are just the parameter scaling factors in the first and second subsystems, respectively.

In addition to the parameter scaling factors, one can also obtain the orbital scaling factors. To look for simple scaling in the phase space at the bicritical point $(A_n^*,B_n^*)$ of level $n$, we first locate the most rarefied region by choosing a $2^n$-periodic orbit point $\mathbf{z}^{(n)}(0)$ that has the largest distance from its nearest orbit point $\mathbf{z}^{(n)}(2^{n-1})$ $[=P^{2^{n-1}}(\mathbf{z}(0))]$. Then, the local rescaling factors of the state variables are simply given by

$$\alpha_{x_1,n}=\frac{d_{x_1,n}}{d_{x_1,n+1}},\quad \alpha_{y_1,n}=\frac{d_{y_1,n}}{d_{y_1,n+1}}, \tag{19a}$$

$$\alpha_{x_2,n}=\frac{d_{x_2,n}}{d_{x_2,n+1}},\quad \alpha_{y_2,n}=\frac{d_{y_2,n}}{d_{y_2,n+1}}, \tag{19b}$$

where

$$d_{x_1,n}\equiv x_1^{(n)}(0)-x_1^{(n)}(2^{n-1}),\quad d_{y_1,n}\equiv y_1^{(n)}(0)-y_1^{(n)}(2^{n-1}), \tag{20a}$$

$$d_{x_2,n}\equiv x_2^{(n)}(0)-x_2^{(n)}(2^{n-1}),\quad d_{y_2,n}\equiv y_2^{(n)}(0)-y_2^{(n)}(2^{n-1}). \tag{20b}$$

As $n\to\infty$, both the rescaling factors $\alpha_{x_1,n}$ and $\alpha_{y_1,n}$ of level $n$ converge to the orbital scaling factor $\alpha_1$ in the first subsystem, while $\alpha_{x_2,n}$ and $\alpha_{y_2,n}$ converge to the orbital scaling factor $\alpha_2$ in the second subsystem.

Using the above residue-matching RG method, we make a numerical analysis of the bicritical scaling behavior and thus obtain the bicritical point, the parameter and orbital scaling factors, and the critical residues. The numerical accuracy is improved remarkably with increasing level $n$. These RG results will be given in Sec. IV along with the scaling results obtained by the direct numerical method.

## IV. SCALING BEHAVIORS NEAR THE BICRITICAL POINTS

In this section, by varying the two control parameters $A$ and $B$ of the two subsystems for a fixed value of the coupling parameter $C$, we study the bicritical scaling behaviors in the two unidirectionally coupled PFPs with $\beta=1.0$ and $\Omega=0.5$. When crossing a bicritical point corresponding to a border of chaos in both subsystems, a transition to hyperchaos occurs, i.e., a hyperchaotic attractor with two positive Lyapunov exponents appears. Since an infinite series of period-doubling transitions to chaos occur successively with increasing amplitude $A$ of the first drive subsystem [16], the unidirectionally coupled PFPs also may exhibit multiple period-doubling transitions to hyperchaos. Here we investigate the first three period-doubling transitions to hyperchaos. For each transition to hyperchaos, various bicritical scaling behaviors are investigated by using both the residue-matching RG method and the direct numerical method. A new type of non-

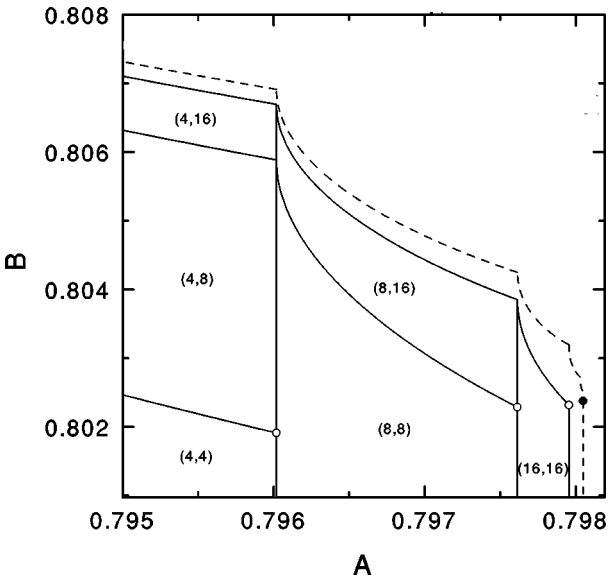


FIG. 1. First stability diagram of asymmetric periodic orbits born via period-doubling bifurcations for $C=-0.2$. Each stable region is labeled by a pair of numbers $(q_1,q_2)$, where $q_1$ and $q_2$ are the periods of oscillations in the first and second subsystems, respectively. When crossing the vertical and nonvertical dashed lines, transitions to chaos occur in the first and second subsystems, respectively. Note that these two critical lines meet at the first bicritical point, denoted by the solid circle, which corresponds to a border of chaos in both subsystems. Furthermore, the open circles denote the points corresponding to a threshold of instability in both subsystems, where $R_1=1$ and $R_2=1$. Such open circles also accumulate to the first bicritical point.

Feigenbaum scaling behaviors are thus found in the second response subsystem. To examine the universality of the bicriticality, we also study several different types of unidirectional couplings. Note that these bicritical scaling behaviors are the same as those in the unidirectionally coupled 1D maps [7,8].

We now fix the coupling parameter as $C=-0.2$, and study period-doubling bifurcations by increasing $B$ from zero. Hence the periodic orbits that exist from $B=0$ become the ''mother'' orbits for such period-doubling cascades. These mother orbits are orbits of type ''$0_s$,'' because they are in-phase (phase shift $N=0$) and consist of the same pairs when coming to $A=B$ and $C=0$ (refer to Sec. II for type of orbits).

Figure 1 shows the first stability diagram of asymmetric periodic orbits. Each stable region is labeled by a pair of numbers $(q_1,q_2)$, where $q_1$ and $q_2$ are the periods of oscillations in the first and second subsystems, respectively. Like the case of the uncoupled PFP [16], as the parameter $A$ is increased, the stationary point $(\hat{x}_1,\hat{y}_1)$ $[=(0,0)]$ in the first subsystem, which is a symmetric one with respect to the inversion operation, becomes unstable through a symmetry-conserving period-doubling bifurcation, and then a new symmetric orbit with period 2 is born. However, the symmetric period-2 orbit loses its stability via a symmetry-breaking pitchfork bifurcation, which leads to the birth of a conjugate pair of asymmetric orbits with period 2. After this breakdown of the inversion symmetry, the first subsystem exhibits an infinite sequence of period-doubling bifurcations at the vertical straight lines in Fig. 1, where $R_1=1$, accumulating at a critical line, denoted by a vertical dashed line. When crossing the vertical critical line, a transition to chaos occurs in the first subsystem. For small values of the parameter $B$, the second subsystem exhibits a forced response with the same period of the first subsystem. As $B$ is increased for a fixed value of $A$, the second subsystem also undergoes an infinite sequence of period-doubling bifurcations at the nonvertical lines, where $R_2=1$, accumulating at a critical line, denoted by a nonvertical dashed line. When crossing the nonvertical critical line, a transition to chaos takes place in the second subsystem. Note that the two critical lines meet at a bicritical point, denoted by a solid circle, corresponding to a threshold of chaos in both the subsystems. Consequently,

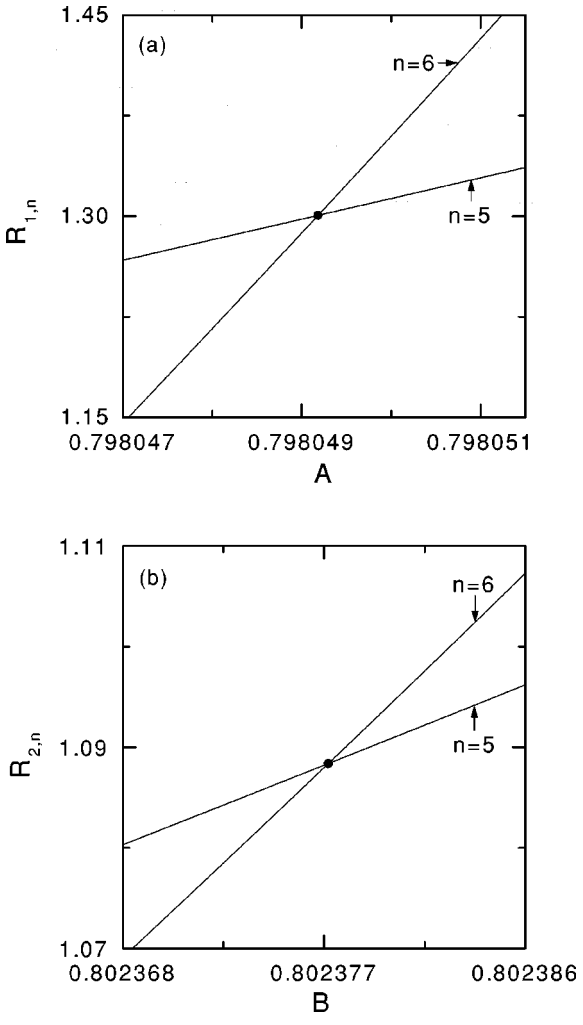


FIG. 2. Plots of (a) the first residue $R_{1,n}(A)$ versus $A$ and (b) the second residue $R_{2,n}(A_5^*,B)$ versus $B$ for the cases $n=5,6$. In (a), the intersection point, denoted by the solid circle, of the two curves $R_{1,5}$ and $R_{1,6}$ gives the point $(A_5^*,R_{1,5}^*)$ of level 5. As $n\to\infty$, $(A_n^*,R_{1,n}^*)$ converges to its limit point $(A^*,R_1^*)$. Similarly, in (b), the intersection point, denoted also by the solid circle, of the two successive curve $R_{2,5}(A_5^*,B)$ and $R_{2,6}(A_5^*,B)$ gives the point $(B_5^*,R_{2,5}^*)$ of level 5. As $n\to\infty$, $(B_n^*,R_{2,n}^*)$ also approaches its limit point $(B^*,R_2^*)$.

TABLE I. Sequences of the critical point, the first critical residue, the parameter, and orbital scaling factors $\{A_n^*\}$, $\{R_{1,n}^*\}$, $\{\delta_{1,n}\}$, $\{\alpha_{x_1,n}\}$, and $\{\alpha_{y_1,n}\}$ in the first subsystem obtained by the residue-matching RG method.

| $n$ | $A_n^*$ | $R_{1,n}^*$ | $\delta_{1,n}$ | $\alpha_{x_1,n}$ | $\alpha_{y_1,n}$ |
|---|---|---|---|---|---|
| 3 | 0.798 049 141 319 | 1.300 47 | 4.672 271 | −2.440 | −2.337 |
| 4 | 0.798 049 183 564 | 1.300 61 | 4.668 814 | −2.530 | −2.573 |
| 5 | 0.798 049 182 420 | 1.300 59 | 4.669 250 | −2.492 | −2.476 |
| 6 | 0.798 049 182 454 | 1.300 60 | 4.669 195 | −2.507 | −2.514 |
| 7 | 0.798 049 182 451 | 1.300 60 | 4.669 202 | −2.501 | −2.499 |
| 8 | 0.798 049 182 452 | 1.300 60 | 4.669 201 | −2.504 | −2.505 |
| 9 | 0.798 049 182 451 | 1.300 59 | 4.669 203 | −2.503 | −2.502 |

when crossing the bicritical point, a hyperchaotic attractor with two positive Lyapunov exponents appears. This is the first transition to hyperchaos. On further increasing $A$, multiple transitions to hyperchaos occur. As examples, second and third transitions to hyperchaos will be also discussed below.

Employing the residue-matching RG method developed in Sec. III, we make an analysis of the scaling behavior near the first bicritical point. Figure 2 shows some RG results obtained by matching the residues of intermediate level $n=5,6$. Plots of the first residue $\mathcal{R}_{1,n}(A)$ versus $A$ for the cases of $n=5,6$ are shown in Fig. 2(a). Note that the intersection point, denoted by the solid circle, of the two curves $\mathcal{R}_{1,5}(A)$ and $\mathcal{R}_{1,6}(A)$ gives the point $(A_5^*,\mathcal{R}_{1,5}^*)$, where $A_5^*$ and $\mathcal{R}_{1,5}^*$ are the critical point and critical residue of level 5 in the first subsystem, respectively. As shown in Eq. (18a), the ratio of the slopes of the curves, $\mathcal{R}_{1,5}$ and $\mathcal{R}_{1,6}$, for $A=A_5^*$ gives the parameter scaling factor $\delta_{1,5}$ of level 5 in the first subsystem. Similarly, Fig. 2(b) shows plots of the second residue $\mathcal{R}_{2,n}(A_5^*,B)$ versus $B$ for the cases of $n=5,6$. The intersection point, denoted also by the solid circle, of the two curves $\mathcal{R}_{2,5}(A_5^*,B)$ and $\mathcal{R}_{2,6}(A_5^*,B)$ gives the point $(B_5^*,\mathcal{R}_{2,5}^*)$, where $B_5^*$ and $\mathcal{R}_{2,5}^*$ are the critical point and critical residue of level 5 in the second subsystem, respectively. As shown in Eq. (18b), the ratio of the slopes of the curves $\mathcal{R}_{2,5}(A_5^*,B)$ and $\mathcal{R}_{2,6}(A_5^*,B)$ for $B=B_5^*$ gives the parameter scaling factor $\delta_{2,5}$ of level 5 in the second subsystem. Increasing the level up to $n=9$, we first solve Eq. (12) to obtain the bicritical point $(A_n^*,B_n^*)$ of level $n$ and a pair of critical residues $(\mathcal{R}_{1,n}^*,\mathcal{R}_{2,n}^*)$ of level $n$. Next, using Eqs. (18) and (19), we obtain the parameter and orbital scaling factors of level $n$, respectively. Then, as the level $n$ is increased, the sequences of the critical points, critical residues, and parameter and orbital scaling factors of level $n$ converge to their respective limit values.

The RG results for the first drive subsystem are listed in Table I. As $n$ is increased, the sequence of the parameter scaling factor $\delta_{1,n}$ converges to a limit value $\delta_1$ ($\simeq 4.669$), and the sequences of the orbital scaling factors $\alpha_{x_1,n}$ and $\alpha_{y_1,n}$ approach the same limit value $\alpha_1$ ($\simeq -2.5$), as in the single PFP [16]. Note that these limit values $\delta_1$ and $\alpha_1$ agree well with Feigenbaum constants $\delta$ ($=4.669\ldots$) and $\alpha$ ($=-2.502\ldots$) for the 1D maps, respectively [1]. With increasing $n$, the sequence of the critical residue $\mathcal{R}_{1,n}^*$ also converges to a limit value $\mathcal{R}^*$ ($\simeq 1.3006$). As shown in Eq. (5), the determinant $\mathcal{D}_1$ of the linearized-map matrix $M_1$ for the $q$-periodic ($q=2^n$) orbit of level $n$ goes to zero as $n\to\infty$. Then, one can easily see from Eq. (7) that the pair of critical Floquet multipliers $(\lambda_{1,1}^*,\lambda_{1,2}^*)$ becomes $(1-2R_1^*,0)$. Note also that the value of $\lambda_{1,1}^*$ ($\simeq -1.601$) agrees well with the 1D critical Floquet multiplier $\lambda^*$ ($=-1.601\ldots$) [1]. Consequently, the first drive subsystem becomes in the usual Feigenbaum critical state.

However, the scaling behavior in the second response subsystem exhibits a new type of non-Feigenbaum scaling behavior, as shown in Table II. As $n$ is increased, the sequence of the parameter scaling factor $\delta_{2,n}$ approaches a

TABLE II. Sequences of the critical point, the second critical residue, the parameter, and orbital scaling factors $\{B_n^*\}$, $\{R_{2,n}^*\}$, $\{\delta_{2,n}\}$, $\{\alpha_{x_2,n}\}$, and $\{\alpha_{y_2,n}\}$ in the second subsystem obtained by the residue-matching RG method.

| $n$ | $B_n^*$ | $R_{2,n}^*$ | $\delta_{2,n}$ | $\alpha_{x_2,n}$ | $\alpha_{y_2,n}$ |
|---|---|---|---|---|---|
| 3 | 0.802 336 15 | 1.071 2 | 2.437 | −1.59 | −1.51 |
| 4 | 0.802 372 86 | 1.084 6 | 2.407 | −1.57 | −1.62 |
| 5 | 0.802 377 20 | 1.088 4 | 2.403 | −1.50 | −1.47 |
| 6 | 0.802 377 13 | 1.088 2 | 2.403 | −1.53 | −1.55 |
| 7 | 0.802 377 10 | 1.088 1 | 2.395 | −1.50 | −1.49 |
| 8 | 0.802 377 24 | 1.089 7 | 2.394 | −1.51 | −1.52 |
| 9 | 0.802 377 21 | 1.089 0 | 2.393 | −1.50 | −1.50 |

limit value $\delta_2(\simeq 2.39)$, and the sequences of the orbital scaling factors $\alpha_{x_2,n}$ and $\alpha_{y_2,n}$ converge to the same limit value $\alpha_2(\simeq -1.5)$. Note that these limit values $\delta_2$ and $\alpha_2$ agree well with the scaling factors $\delta_2(=2.392\ldots)$ and $\alpha_2(=-1.505\ldots)$ in the second response subsystem for the unidirectionally-coupled 1D maps, respectively [7,8]. With increasing $n$, the sequence of the critical residue $\mathcal{R}^*_{2,n}$ also converges to a limit value $\mathcal{R}^*(\simeq 1.089)$, and hence the corresponding pair of critical Floquet multipliers $(\lambda^*_{2,1},\lambda^*_{2,2})$ becomes $(1-2R^*_2,0)$ $[\simeq(-1.178,0)]$. Here the value of $\lambda^*_{2,1}$ also agrees well with the second critical Floquet multiplier $\lambda^*_2$ $(=-1.178\ldots)$ in the second response subsystem for the unidirectionally coupled 1D maps [7,8]. Consequently, the bicritical scaling behavior in the unidirectionally coupled PFPs becomes the same as that in the unidirectionally coupled 1D maps.

To confirm the RG results, we also investigate the bicritical scaling behaviors by the direct numerical method. Consider a pair of the parameters $(A_n,B_n)$ at which the periodic orbit of level $n$ (period $2^n$) has the residues $R_{1,n}=R_{2,n}=1$. Note that the point $(A_n,B_n)$ corresponds to a threshold of instability in both subsystems. Some of such points are denoted by open circles in Fig. 1. Then the sequence of $(A_n,B_n)$ converges to the first bicritical point $(A_c^{(1)},B_c^{(1)})$, denoted by the solid circle, as the level $n$ is increased. To locate the first bicritical point with a satisfactory precision, we directly follow the orbits of period $2^n$ up to level $n=10$, and obtain the sequences of both the parameters $(A_n,B_n)$ and the orbit points $\mathbf{z}_n[=(z_{1,n},z_{2,n})]$ that has the maximum distance from its nearest orbit point, where $z_{i,n}=(x_{i,n},y_{i,n})$ $(i=1,2)$.

The asymptotic scaling behaviors of the above sequences near the first bicritical point are investigated in both subsystems. Note that the scaling behavior in the first drive subsystem is obviously the same as that in the uncoupled PFP [16]. Hence, as in the uncoupled PFP, the sequences $\{A_n\}$, $\{x_{1,n}\}$, and $\{y_{1,n}\}$ converge to their limit values $A_c^{(1)}$ $(=0.798\,049\,182\,45)$, $x_1^*(=0.100\,545\,5)$, $y_1^*(=0.567\,171)$ geometrically with the 1D asymptotic ratios, respectively,

$$A_n-A_c^{(1)}\sim\delta_1^{-n},\quad x_{1,n}-x_1^*\sim\alpha_1^{-n},\quad y_{1,n}-y_1^*\sim\alpha_1^{-n}. \tag{21}$$

Here the limit values are obtained using the superconverging method [24], and the scaling factors $\delta_1$ and $\alpha_1$ are just the Feigenbaum constants $\delta(=4.669\ldots)$ and $\alpha(=-2.502\ldots)$, for the 1D maps, respectively. However, the second response subsystem exhibits a non-Feigenbaum scaling behavior. The sequences $\{B_n\}$, $\{x_{2,n}\}$, and $\{y_{2,n}\}$ also converge geometrically to their limit values $B_c^{(1)}$ $(=0.802\,377)$, $x_2^*(=0.100\,111)$, $y_2^*(=0.568\,65)$, respectively, where the limit values are also obtained using the superconverging method. To get the convergence rates of the sequences, we define the scaling factors of level $n$,

$$\delta_{2,n}\equiv\frac{B_{n-1}-B_n}{B_n-B_{n+1}},\quad \alpha_{x_2,n}\equiv\frac{x_{2,n-1}-x_{2,n}}{x_{2,n}-x_{2,n+1}}, \tag{22}$$

TABLE III. Sequences of the parameter and orbital scaling factors $\{\delta_{2,n}\}$, $\{\alpha_{x_2,n}\}$, and $\{\alpha_{y_2,n}\}$ in the second subsystem obtained by directly following the ''self-similar'' parameter and orbital sequences.

| $n$ | $\delta_{2,n}$ | $\alpha_{x_2,n}$ | $\alpha_{y_2,n}$ |
|---|---|---|---|
| 4 | 1.035 | −1.548 | −1.571 |
| 5 | 1.836 | −1.511 | −1.495 |
| 6 | 2.475 | −1.511 | −1.522 |
| 7 | 2.543 | −1.506 | −1.499 |
| 8 | 2.273 | −1.506 | −1.511 |
| 9 | 2.474 | −1.505 | −1.502 |

$$\alpha_{y_2,n}\equiv\frac{y_{2,n-1}-y_{2,n}}{y_{2,n}-y_{2,n+1}}.$$

The sequence $\{\delta_{2,n}\}$ is listed in Table III, and it seems to converge to a limit value $\delta_2(\sim 2.4)$, which confirms the RG result of $\delta_2$ $(\simeq 2.39)$. Both the sequences $\{\alpha_{x_2,n}\}$ and $\{\alpha_{y_2,n}\}$ also seem to approach the same limit $\alpha_2$ $(\simeq -1.5)$, which also agrees well with the RG result of $\alpha_2$ $(\simeq -1.5)$.

To demonstrate the parameter scaling, we study the ''topography'' of the parameter plane. Figure 3 shows the phase diagrams near the first bicritical point $(A_c^{(1)},B_c^{(1)})$. States in

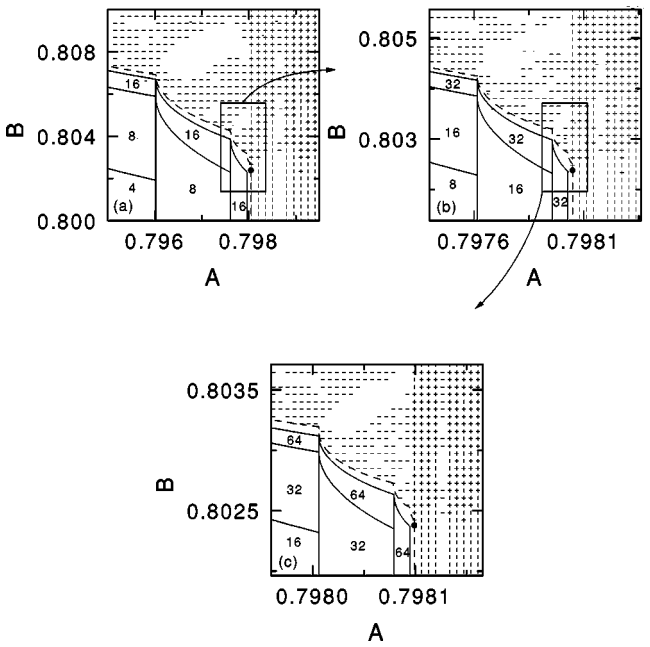


FIG. 3. Phase diagrams near the first bicritical point $(A_c^{(1)},B_c^{(1)})$ for $C=-0.2$. States in the parameter plane are determined by their Lyapunov exponents. White areas correspond to periodic states and the numbers denote the periods. Vertical and horizontal dashes denote chaotic states in the first and second subsystems, respectively, and crosses correspond to hyperchaotic states with two positive Lyapunov exponents. The pictures in (b) and (c) are obtained by magnifying the regions in the small boxes in the previous pictures by the scaling factor $\delta_1$ for the $A$ axis and $\delta_2$ for the $B$ axis. Each successive picture reproduces the previous one with an accuracy increasing with the depth of resolution.

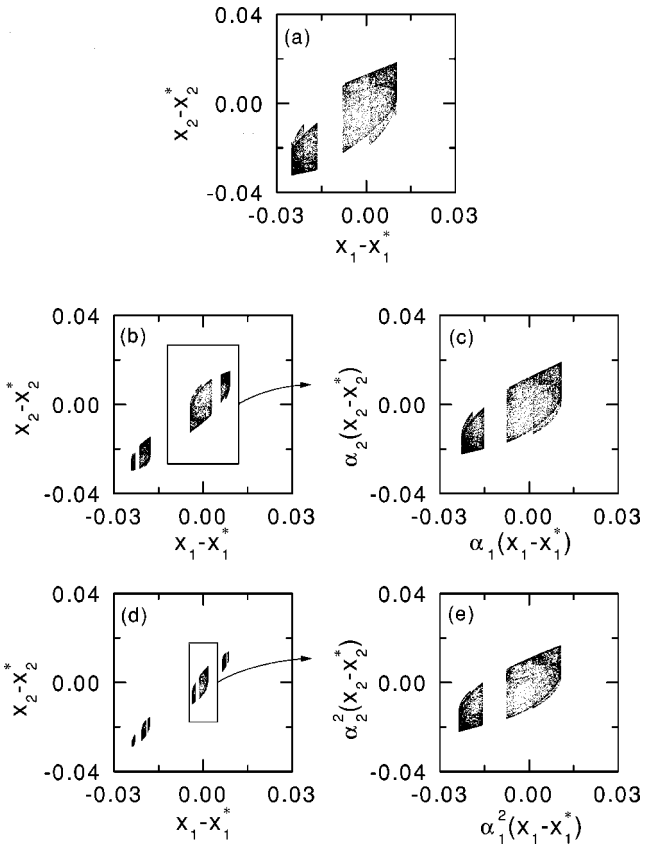


FIG. 4. Hyperchaotic attractors for the three values of $(A,B)$ near the first bicritical point $(A_c^{(1)},B_c^{(1)})$ for $C=-0.2$; in (a) $(A,B)=(A_c^{(1)}+\Delta A,B_c^{(1)}+\Delta B)$ $(\Delta A=0.000\,85,\Delta B=0.0037)$, in (b) and (c) $(A,B)=(A_c^{(1)}+\Delta A/\delta_1,B_c^{(1)}+\Delta B/\delta_2)$, and in (d) and (e) $(A,B)=(A_c^{(1)}+\Delta A/\delta_1^2,B_c^{(1)}+\Delta B/\delta_2^2)$. The picture in (c) is obtained by magnifying the region in the small box in (b) with the scaling factors $\alpha_1$ for the $x_1$ axis and $\alpha_2$ for the $x_2$ axis. Similarly, we also obtain the picture (e) by magnifying the region inside the small box in (d) with the scaling factors $\alpha_1^2$ for the $x_1$ axis and $\alpha_2^2$ for the $x_2$ axis. Comparing the pictures in (a), (c), and (e), one can see that each successive magnified picture reproduces the previous one with an accuracy with the depth of resolution.

the parameter plane are determined by calculating their Lyapunov exponents. White areas correspond to periodic states and the numbers denote the periods. On the other hand, vertical and horizontal dashes denote chaotic states in the first and second subsystems, respectively, and crosses correspond to hyperchaotic states with two positive Lyapunov exponents. The pictures in Figs. 3(b) and 3(c) are obtained by magnifying the regions in the small boxes in the previous pictures by the scaling factor $\delta_1$ for the $A$ axis and $\delta_2$ for the $B$ axis. Note that each successive picture reproduces the previous one with an accuracy increasing with the depth of resolution. Hence the configuration of states in Fig. 3 demonstrates the parameter scaling near the bicritical point.

For another evidence of scaling, we also compare the hyperchaotic attractors, shown in Fig. 4, for the three values of $(A,B)$ near the first bicritical point $(A_c^{(1)},B_c^{(1)})$. Figure 4(a) shows the 2D projection of a hyperchaotic attractor onto the $x_1$-$x_2$ plane with the origin shifted at $(x_1^*,x_2^*)$ for $A=A_c^{(1)}+\Delta A$ and $B=B_c^{(1)}+\Delta B$, where $\Delta A=0.000\,85$ and $\Delta B=0.0037$. This hyperchaotic attractor has two positive Lyapunov exponents, $\sigma_{1,1}\simeq 0.107$ and $\sigma_{2,1}\simeq 0.045$. To see scaling, we first rescale $\Delta A$ and $\Delta B$ with the parameter scaling factors $\delta_1$ and $\delta_2$, respectively. The 2D projection of the attractor for the rescaled parameter values of $A=A_c^{(1)}+\Delta A/\delta_1$ and $B=B_c^{(1)}+\Delta B/\delta_2$ is shown in Fig. 4(b). It is also the hyperchaotic attractor with $\sigma_1\simeq 0.055$ and $\sigma_2\simeq 0.023$. We next magnify the region in the small box (containing the origin) by the scaling factor $\alpha_1$ for the $x_1$ axis and $\alpha_2$ for the $x_2$ axis, and then we get the magnified picture in Fig. 4(c). Note that the picture in Fig. 4(c) reproduces the previous one in Fig. 4(a) approximately. Repeating the above procedure once more, we obtain the two pictures in Figs. 4(d) and 4(e). That is, Fig. 4(d) shows the hyperchaotic attractor with $\sigma_1\simeq 0.027$ and $\sigma_2\simeq 0.012$ for $A=A_c^{(1)}+\Delta A/\delta_1^2$ and $B=B_c^{(1)}+\Delta B/\delta_2^2$. Magnifying the region in the small box with the scaling factors $\alpha_1^2$ for the $x_1$ axis and $\alpha_2^2$ for the $x_2$ axis, we also obtain the magnified picture in Fig. 4(e), which reproduces the previous one in Fig. 4(c) with an increased accuracy.

We now turn to a brief discussion of the behavior exactly at the first bicritical point $(A_c^{(1)},B_c^{(1)})$. There exist infinite unstable periodic orbits with period $2^n$, forming the skeleton of the bicritical attractor. The orbit points $z_{1,n}$ and $z_{2,n}$ that have the maximum distances from their nearest orbit points in the first and second subsystems are found to converge geometrically to their limit points $z_1^*$ and $z_2^*$ with the asymptotic ratios $\alpha_1$ and $\alpha_2$, respectively. The residues $R_{1,n}$ and $R_{2,n}$ of the orbits with period $2^n$ are also found to converge to the critical residues $R_1^*$ and $R_2^*$, respectively.

With further increase of $A$ from its first critical point $A_c^{(1)}$, the stationary point $(\hat{x}_1,\hat{y}_1)$ $[=(0,0)]$ in the first subsystem undergoes a cascade of ''resurrections,'' i.e., it becomes restabilized after it loses its stability, destabilizes again and so forth *ad infinitum*. (For detail on such resurrections, refer to Ref. [16].) For each case of the resurrections, an infinite sequence of period-doubling bifurcations follows after breakdown of the inversion symmetry. Consequently, the unidirectionally coupled PFPs exhibit multiple transitions to hyperchaos. As examples, we investigate the scaling behaviors associated with the second and third transitions to hyperchaos. Figure 5 shows the second and third stability diagrams of asymmetric periodic orbits. Each stable region is labeled by a pair of numbers $(q_1,q_2)$, where $q_1$ and $q_2$ are the periods of oscillations in the first and second subsystems, respectively. When crossing the vertical (nonvertical) critical line, denoted by a dashed line, a transition to chaos occurs in the first (second) subsystem. Note that the critical lines in Figs. 5(a) and 5(b) meet at the second and third bicritical points $(A_c^{(2)},B_c^{(2)})$ and $(A_c^{(3)},B_c^{(3)})$, where $(A_c^{(2)},B_c^{(2)})=(3.501\,110\,775,3.518\,32)$ and $(A_c^{(3)},B_c^{(3)})=(10.508\,324\,894\,38,10.534\,88)$, respectively. The scaling behaviors near these bicritical points are found to be the same as those near the first bicritical point.

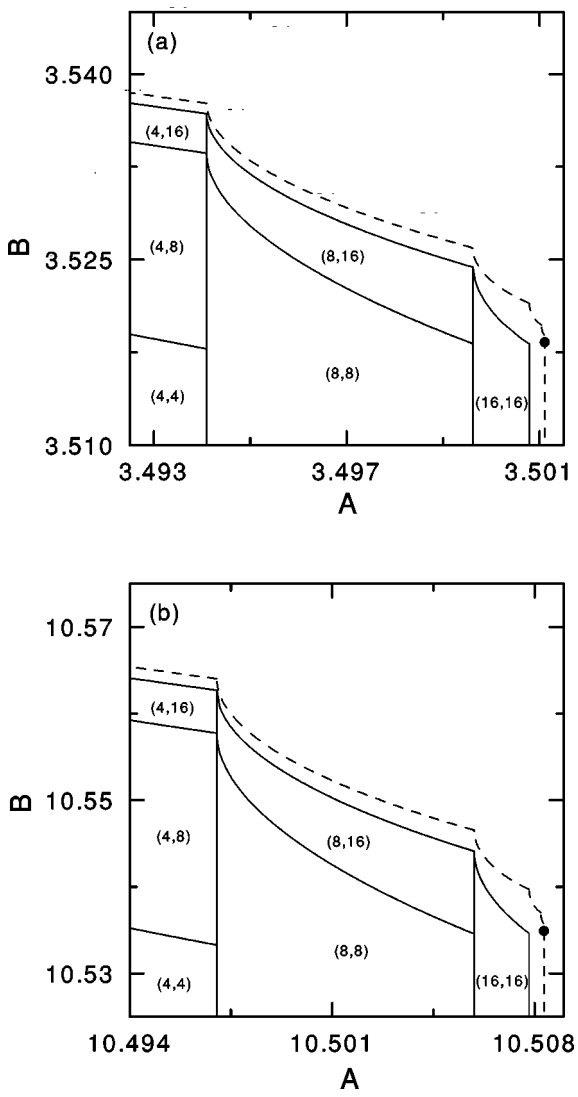


FIG. 5. (a) Second and (b) third stability diagrams of asymmetric periodic orbits for $C=-0.2$. Here each stable region is labeled by a pair of numbers $(q_1,q_2)$, where $q_1$ and $q_2$ denote the periods of oscillations in the first and second subsystems, respectively. The (vertical and nonvertical) critical lines, denoted by dashed lines in (a) and (b), of period-doubling transitions to chaos in both subsystems meet at the second and third bicritical points, denoted by the solid circles, respectively. Note that the structure of these second and third stability diagrams is the same as that of the first stability diagram.

To examine universality in the bicritical behavior, we also consider a system consisting of two PFPs with a unidirectional coupling of general type, described by

$$\dot{x}_1=y_1, \tag{23a}$$

$$\dot{y}_1=f_A(x_1,y_1,t), \tag{23b}$$

$$\dot{x}_2=y_2+g_1(x_1,y_1,x_2,y_2), \tag{23c}$$

$$\dot{y}_2=f_B(x_2,y_2,t)+g_2(x_1,y_1,x_2,y_2), \tag{23d}$$

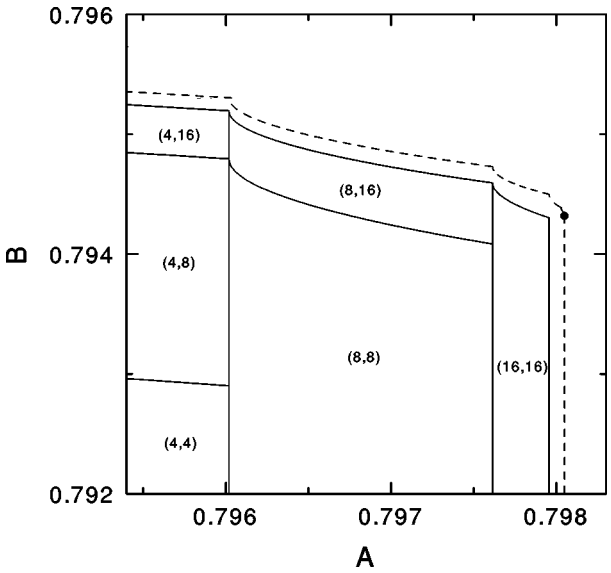


FIG. 6. First stability diagram of asymmetric periodic orbits for the fourth type of coupling with $g_1=0$ and $g_2=C(x_2-x_1)$ for $C=-0.1$. Here each stable region is labeled by a pair of numbers $(q_1,q_2)$, where $q_1$ and $q_2$ denote the periods of oscillations in the first and second subsystems, respectively. The two (vertical and non-vertical) critical lines, denoted by the dashed lines, of period-doubling transitions to chaos meet at the bicritical point, denoted by the solid circle. Note that the structure of this stability diagram is the same as that of the first stability diagram for the first type of coupling.

where $f_A(x,y,t)=-2\pi\beta\Omega y-2\pi(\Omega^2-A\cos 2\pi t)\sin 2\pi x$, and $A$ and $B$ are the control parameters of the two subsystems. For this unidirectionally coupled system, the first PFP with state variables $x_1$ and $y_1$ is a master subsystem driving the second slave or response PFP with state variables $x_2$ and $y_2$ through the generalized coupling terms $g_1$ and $g_2$. The bicritical behaviors are investigated for the cases of the following six types of couplings:

$$g_1=C(x_2-x_1),\quad g_2=C(y_2-y_1), \tag{24a}$$

$$g_1=C(x_2-x_1),\quad g_2=0, \tag{24b}$$

$$g_1=0,\quad g_2=C(y_2-y_1), \tag{24c}$$

$$g_1=0,\quad g_2=C(x_2-x_1), \tag{24d}$$

$$g_1=C(x_2^2-x_1^2),\quad g_2=C(y_2^2-y_1^2), \tag{24e}$$

$$g_1=C(x_2^3-x_1^3),\quad g_2=C(y_2^3-y_1^3), \tag{24f}$$

where $C$ is a coupling parameter. [Here the first type of coupling is just the coupling considered in Eq. (2).] It is thus found that the scaling behaviors near the bicritical points are the same irrespective of the type of couplings although the type of mother orbits for the period-doubling cascades depends on the type of couplings. As an example, consider the fourth type of coupling in Eq. (24d). Figure 6 shows the first stability diagram of asymmetric periodic orbits for $C=-0.1$. We first note the ''universal'' structure of the stability

diagram. The scaling behavior near the bicritical point is found to be the same as that for the first type of coupling although the type of mother orbits is different from that for the first type of coupling. For this case, the type of mother orbits that exist from $B=0$ is ''$1_s$'' because they are out-of-phase orbits with phase shift $N=1$ and consist of the same pairs when coming to $A=B$ and $C=0$ (refer to Sec. II for type of orbits).

## V. SUMMARY

We have studied the bicritical scaling behavior of period doublings in two unidirectionally coupled PFPs. When crossing a bicritical point corresponding to a threshold of chaos in both subsystems, a hyperchaotic attractor with two Lyapunov exponents appears, i.e., a transition to hyperchaos occurs. Varying the control parameters of both subsystems, the unidirectionally coupled PFPs exhibit a cascade of transitions to hyperchaos. Using both the residue-matching RG method and the direct numerical method, we have investigated scaling behaviors near the bicritical points for several cases of unidirectional couplings and found a new kind of non-Feigenbaum scaling behavior in the response subsystem. Note also that this bicritical scaling behavior is the same as that in the unidirectionally coupled 1D maps. We thus suppose that the bicriticality may occur generally in a large class of unidirectionally coupled systems consisting of period-doubling subsystems.

## ACKNOWLEDGMENT

This work was supported by the Korea Research Foundation under Grant No. KRF-99-041-D00123.

[1] M.J. Feigenbaum, J. Stat. Phys. **19**, 25 (1978); **21**, 669 (1979).
[2] P. Collet, J.-P. Eckmann, and H. Koch, J. Stat. Phys. **25**, 1 (1981).
[3] S.P. Kuznetsov, Radiophys. Quantum Electron. **28**, 681 (1985); S.P. Kuznetsov and A.S. Pikovsky, Physica D **19**, 384 (1986).
[4] S.-Y. Kim and H. Kook, Phys. Rev. A **46**, R4467 (1992); Phys. Lett. A **178**, 258 (1993); Phys. Rev. E **48**, 785 (1993); S.-Y. Kim, *ibid.* **54**, 3393 (1996).
[5] S.-Y. Kim and K. Lee, Phys. Rev. E **54**, 1237 (1996); S.-Y. Kim and B. Hu, *ibid.* **58**, 7231 (1998).
[6] I. Waller and R. Kapral, Phys. Rev. A **30**, 2047 (1984); H. Kook, F.H. Ling, and G. Schmidt, *ibid.* **43**, 2700 (1991).
[7] A.P. Kuznetsov, S.P. Kuznetsov, and I.R. Sataev, Int. J. Bifurcation Chaos Appl. Sci. Eng. **1**, 839 (1991); Physica D **109**, 91 (1997).
[8] S.-Y. Kim, Phys. Rev. E **59**, 6585 (1999).
[9] B.P. Bezruchko, V.Yu. Gulyaev, S.P. Kuznetsov, and E.P. Seleznev, Sov. Phys. Dokl. **31**, 268 (1986) [Dokl. Akad. Nauk SSSR **287**, 619 (1986)]; A.P. Kuznetsov, S.P. Kuznetsov, and I.R. Saraev, Int. J. Bifurcation Chaos Appl. Sci. Eng. **6**, 119 (1996).
[10] K. Kaneko, Phys. Lett. **111A**, 321 (1985); I.S. Aranson, A.V. Gaponov-Grekhov, and M.I. Rabinovich, Physica D **33**, 1 (1988); F.H. Willeboordse and K. Kaneko, Phys. Rev. Lett. **73**, 533 (1994); Physica D **86**, 428 (1995); O. Rudzick and A. Pikovsky, Phys. Rev. E **54**, 5107 (1996).
[11] J.H. Xiao, G. Hu, and Z. Qu, Phys. Rev. Lett. **77**, 4162 (1996); Y. Zhang, G. Hu, and L. Gammaitoni, Phys. Rev. E **58**, 2952 (1998); M. Hasler, Int. J. Bifurcation Chaos Appl. Sci. Eng. **8**, 647 (1998).
[12] T. Kapitaniak and L.O. Chua, Int. J. Bifurcation Chaos Appl. Sci. Eng. **4**, 477 (1994).
[13] G. Santoboni, S.R. Bishop, and A. Varone, Int. J. Bifurcation Chaos Appl. Sci. Eng. **12**, 2345 (1999).
[14] K.M. Campbell and M.E. Davies, Nonlinearity **9**, 801 (1996); K.M. Campbell, Physica D **107**, 43 (1997).
[15] L.D. Landau and E.M. Lifshitz, *Mechanics* (Pergamon Press, New York, 1976), p. 80; V.I. Arnold, *Mathematical Methods of Classical Mechanics* (Springer-Verlag, New York, 1978), p. 113.
[16] S.-Y. Kim and K. Lee, Phys. Rev. E **53**, 1579 (1996).
[17] O.E. Rössler, Phys. Lett. **71A**, 155 (1979); K. Kaneko, Prog. Theor. Phys. **69**, 1427 (1983); T. Kapitaniak and W.-H. Steeb, Phys. Lett. A **152**, 33 (1991); M. de Sousa Vieira, A.J. Lichtenberg, and M.A. Lieberman, Phys. Rev. A **46**, R7359 (1992); T. Kapitaniak and L.O. Chua, Int. J. Bifurcation Chaos Appl. Sci. Eng. **4**, 477 (1994); M.A. Harrison and Y.-C. Lai, Phys. Rev. E **59**, R3799 (1999).
[18] S.-Y. Kim and B. Hu, Phys. Rev. A **44**, 934 (1991); S.-Y. Kim and D.-S. Lee, *ibid.* **45**, 5480 (1992).
[19] S. Lefschetz, *Differential Equations: Geometric Theory* (Dover, New York, 1977), Sec. 3.5.
[20] V.I. Arnold, *Ordinary Differential Equations* (MIT Press, Cambridge, MA, 1973), p. 114.
[21] J. Guckenheimer and P. Holmes, *Nonlinear Oscillations, Dynamical Systems and Bifurcations of Vector Fields* (Springer-Verlag, New York, 1983), Sec. 3.5.
[22] A.J. Lichtenberg and M.A. Lieberman, *Regular and Stochastic Motion* (Springer-Verlag, New York, 1983), Sec. 5.3.
[23] J.M. Greene, J. Math. Phys. **20**, 1183 (1979); R.S. MacKay, Physica D **7**, 283 (1983).
[24] R. S. MacKay, Ph.D. thesis, Princeton University, 1982. See Eqs. 3.1.2.12 and 3.1.2.13.